SCIENCE CHINA
Information Sciences

• **Supplementary File** •

Performance Guaranteed Adaptive Fault-Tolerant Tracking Control of Six-DOF Spacecraft

Kewei XIA[1] & Yao ZOU[2,3*]

[1]*Yonsei University Observatory, Yonsei University, Seoul* 03722*, Republic of Korea;*
[2]*School of Automation and Electrical Engineering, University of Science and Technology Beijing, Beijing* 100083*, P. R. China;*
[3]*Institute of Artificial Intelligence, University of Science and Technology Beijing, Beijing* 100083*, P. R. China*

Appendix A Six-dof dynamics model

To establish the dynamics of a rigid spacecraft, the following coordinate frames are needed:

• Inertial (earth) frame $\mathcal{F}_I = \{O_I \boldsymbol{x}_I \boldsymbol{y}_I \boldsymbol{z}_I\}$: origin O_I is located at the earth center, axis $\boldsymbol{x}_I$ points to the vernal equinox, axis $\boldsymbol{z}_I$ points to the north pole, and axis $\boldsymbol{y}_I$ is determined by Right-Hand-Rule (RHR).

• Body frame $\mathcal{F}_B = \{O_B \boldsymbol{x}_B \boldsymbol{y}_B \boldsymbol{z}_B\}$: origin O_B coincides with the spacecraft center of mass, and three axes coincide with three inertial principal axes, respectively.

• Local vertical local horizontal (i.e., LVLH) frame $\mathcal{F}_L = \{O_L \boldsymbol{x}_L \boldsymbol{y}_L \boldsymbol{z}_L\}$: origin O_L is situated at the center of the desired target, axis $\boldsymbol{x}_L$ points from the earth center to O_L, axis $\boldsymbol{z}_L$ is perpendicular to the orbit plane, and $\boldsymbol{y}_L$ axis is in the orbit plane and is determined by RHR.

The spacecraft attitude with respect to the inertial frame is represented by modified Rodrigues parameters (MRPs) $\boldsymbol{\sigma} = \hat{\boldsymbol{n}} \tan(\frac{\gamma}{4})$, where $\hat{\boldsymbol{n}} \in \mathbb{S}_2$[1)] and $\gamma \in (-2\pi, 2\pi)$ are the principal rotation axis and angle [1]. According to [1], $\boldsymbol{\sigma}$ satisfies the following kinematics:

$$\dot{\boldsymbol{\sigma}} = \boldsymbol{G}(\boldsymbol{\sigma})\boldsymbol{\omega}, \tag{A1}$$

where $\boldsymbol{G}(\boldsymbol{\sigma}) = \frac{1}{4}\left[(1 - \|\boldsymbol{\sigma}\|^2)\boldsymbol{I}_3 + 2\boldsymbol{\sigma}^\times + 2\boldsymbol{\sigma}\boldsymbol{\sigma}^T\right]$[2)], and $\boldsymbol{\omega} \in \mathbb{R}^3$ is the angular velocity. Moreover, given a desired attitude $\boldsymbol{\sigma}_d$ governed by

$$\dot{\boldsymbol{\sigma}}_d = \boldsymbol{G}(\boldsymbol{\sigma}_d)\boldsymbol{\omega}_d, \tag{A2}$$

with $\boldsymbol{\omega}_d$ being the desired angular velocity, the error MRPs $\tilde{\boldsymbol{\sigma}}$ between $\boldsymbol{\sigma}$ and $\boldsymbol{\sigma}_d$ is defined by

$$\tilde{\boldsymbol{\sigma}} = \frac{\boldsymbol{\sigma}_d(\|\boldsymbol{\sigma}\|^2 - 1) + \boldsymbol{\sigma}(1 - \|\boldsymbol{\sigma}_d\|^2) - 2\boldsymbol{\sigma}_d^\times \boldsymbol{\sigma}}{1 + \|\boldsymbol{\sigma}_d\|^2\|\boldsymbol{\sigma}\|^2 + 2\boldsymbol{\sigma}_d^T\boldsymbol{\sigma}}. \tag{A3}$$

As derived in [1], the kinematics of $\tilde{\boldsymbol{\sigma}}$ satisfies

$$\dot{\tilde{\boldsymbol{\sigma}}} = \boldsymbol{G}(\tilde{\boldsymbol{\sigma}})\tilde{\boldsymbol{\omega}}, \tag{A4}$$

where $\tilde{\boldsymbol{\omega}} = \boldsymbol{\omega} - \tilde{\boldsymbol{R}}\boldsymbol{\omega}_d$ is the angular velocity error. The rotation matrix $\tilde{\boldsymbol{R}} = \tilde{\boldsymbol{R}}(\tilde{\boldsymbol{\sigma}})$ can be represented by

$$\tilde{\boldsymbol{R}}(\tilde{\boldsymbol{\sigma}}) = \boldsymbol{I}_3 - \frac{4(1 - \|\tilde{\boldsymbol{\sigma}}\|^2)}{(1 + \|\tilde{\boldsymbol{\sigma}}\|^2)^2}\tilde{\boldsymbol{\sigma}}^\times + \frac{8(\tilde{\boldsymbol{\sigma}}^\times)^2}{(1 + \|\tilde{\boldsymbol{\sigma}}\|^2)^2}. \tag{A5}$$

Next, according to [1], $\tilde{\boldsymbol{\omega}}$ satisfies the following dynamics:

$$\boldsymbol{J}\dot{\tilde{\boldsymbol{\omega}}} = -\boldsymbol{\omega}^\times \boldsymbol{J}\boldsymbol{\omega} + \boldsymbol{A}_r\boldsymbol{\tau} + \boldsymbol{\tau}_d + \boldsymbol{J}(\tilde{\boldsymbol{\omega}}^\times \tilde{\boldsymbol{R}}\boldsymbol{\omega}_d - \tilde{\boldsymbol{R}}\dot{\boldsymbol{\omega}}_d), \tag{A6}$$

where $\boldsymbol{J} \in \mathbb{R}^{3\times 3}$ is the inertia matrix of the spacecraft, $\boldsymbol{\tau} \in \mathbb{R}^N$ is the control torque stack, $\boldsymbol{A}_r \in \mathbb{R}^{3\times N}$ with $\mathrm{rank}(\boldsymbol{A}_r) = 3$ is the distribution matrix of $N (N \geqslant 3)$ torque actuators, and $\boldsymbol{\tau}_d \in \mathbb{R}^3$ is the disturbed torque.

Define $\boldsymbol{r}$ and $\boldsymbol{v}$ as the position and velocity of the spacecraft in frame $\mathcal{F}_L$. Given a time-varying desired offset $\boldsymbol{\delta}$, we further define the position and velocity errors as $\tilde{\boldsymbol{r}} = \boldsymbol{r} - \boldsymbol{\delta}$ and $\tilde{\boldsymbol{v}} = \boldsymbol{v} - \dot{\boldsymbol{\delta}}$. According to [2, 3], they satisfy the following dynamics:

$$\dot{\tilde{\boldsymbol{r}}} = \tilde{\boldsymbol{v}}, \tag{A7}$$

$$m\dot{\tilde{\boldsymbol{v}}} = -m\boldsymbol{C}_t\boldsymbol{v} - m\boldsymbol{n}_t + \boldsymbol{R}_L^B\boldsymbol{A}_t\boldsymbol{f} + \boldsymbol{f}_d - m\ddot{\boldsymbol{\delta}}, \tag{A8}$$

* Corresponding author (email: zouyao@ustb.edu.cn)

1) $\mathbb{S}_2 = \{x \in \mathbb{R}^3 | \|x\| = 1\}$

2) For $\boldsymbol{x} = [x_1, x_2, x_3]^T$, $\boldsymbol{x}^\times = [0, -x_3, x_2; x_3, 0, -x_1; -x_2, x_1, 0]$

where m is the spacecraft mass,

$$\boldsymbol{C}_t = 2\dot{\nu}\begin{bmatrix} 0 & -1 & 0 \\ 1 & 0 & 0 \\ 0 & 0 & 0 \end{bmatrix},\ \boldsymbol{n}_t = \begin{bmatrix} -\ddot{\nu}r_y - \dot{\nu}^2 r_x + \frac{\mu(r_0+r_x)}{((r_0+r_x)^2+r_y^2+r_z^2)^{\frac{3}{2}}} - \frac{\mu}{r_0^2} \\ \ddot{\nu}r_x - \dot{\nu}^2 r_y + \frac{\mu r_y}{((r_0+r_x)^2+r_y^2+r_z^2)^{\frac{3}{2}}} \\ \frac{\mu r_z}{((r_0+r_x)^2+r_y^2+r_z^2)^{\frac{3}{2}}}] \end{bmatrix},$$

$r_0 = \frac{a(1-e^2)}{1+e\cos\nu}$ is the radial distance between the desired target and the earth, a is the semimajor axis, e is the eccentricity, ν is the true anomaly, $\boldsymbol{R}_L^B = \boldsymbol{R}_L\boldsymbol{R}^T(\boldsymbol{\sigma})$ is the rotation matrix from frame $\mathcal{F}_B$ to frame $\mathcal{F}_L$, $\boldsymbol{R}_L$ is the rotation matrix from frame $\mathcal{F}_I$ to frame $\mathcal{F}_L$, $\boldsymbol{f} \in \mathbb{R}^M$ is the control force stack, $\boldsymbol{A}_t \in \mathbb{R}^{3\times M}$ with $\mathrm{rank}(\boldsymbol{A}_t) = 3$ is the distribution matrix of $M(M \geqslant 3)$ force actuators, and $\boldsymbol{f}_d \in \mathbb{R}^3$ is the disturbed force. Moreover, the rotation matrix $\boldsymbol{R}_L$ is expressed by

$$\boldsymbol{R}_L = \begin{bmatrix} \mathrm{c}(\Omega_0)\mathrm{c}(\theta_0) - \mathrm{s}(\Omega_0)\mathrm{s}(\theta_0)\mathrm{c}(i_0) & \mathrm{s}(\Omega_0)\mathrm{c}(\theta_0) + \mathrm{c}(\Omega_0)\mathrm{s}(\theta_0)\mathrm{c}(i_0) & \mathrm{s}(\theta_0)\mathrm{s}(i_0) \\ -\mathrm{c}(\Omega_0)\mathrm{s}(\theta_0) - \mathrm{s}(\Omega_0)\mathrm{c}(\theta_0)\mathrm{c}(i_0) & -\mathrm{s}(\Omega_0)\mathrm{s}(\theta_0) + \mathrm{c}(\Omega_0)\mathrm{c}(\theta_0)\mathrm{c}(i_0) & \mathrm{c}(\theta_0)\mathrm{s}(i_0) \\ \mathrm{s}(\Omega_0)\mathrm{s}(i_0) & -\mathrm{c}(\Omega_0)\mathrm{s}(i_0) & \mathrm{c}(i_0) \end{bmatrix},$$

where $\mathrm{c}(\cdot) \triangleq \cos(\cdot)$, $\mathrm{s}(\cdot) \triangleq \sin(\cdot)$, Ω_0 is the right ascension of ascending node, $\theta_0 = \omega_p + \nu$ is the argument of latitude, ω_p is the argument of perigee, and i_0 is the orbit inclination.

Consider the torque and force that steer the spacecraft being generated by N momentum wheels and M pairs of thrusters, respectively. In particular, each momentum wheel generates a torque around a specified rotation axis through the origin O_B of frame $\mathcal{F}_B$, while two thrusters assembled symmetrically with respect to O_B generate the positive and opposite forces along their assembling axis. In practice, due to long-term friction, aging and mechanical damage, the actuator is sometimes subject to undesirable fault. In spatial circumstance, it is difficult to repair the actuator manually. Hence, it is favorable to improve the robust performance against the actuator fault from the perspective of the control algorithm. In particular, by taking a general form of actuator fault with both additive and multiplicative fault effects, the resulting torque and force are formulated by

$$\boldsymbol{\tau} = \boldsymbol{\Upsilon}_r\boldsymbol{p}_r + \boldsymbol{\phi}_r,\ \ \boldsymbol{f} = \boldsymbol{\Upsilon}_t\boldsymbol{p}_t + \boldsymbol{\phi}_t, \tag{A9}$$

where $\boldsymbol{p}_r \in \mathbb{R}^N$ and $\boldsymbol{p}_t \in \mathbb{R}^M$ are the command torque and force to be designed, $\boldsymbol{\Upsilon}_r = \mathrm{diag}(\upsilon_{r1}, \upsilon_{r2}, \cdots, \upsilon_{tN})$ and $\boldsymbol{\Upsilon}_t = \mathrm{diag}(\upsilon_{t1}, \upsilon_{t2}, \cdots, \upsilon_{tM})$ are the fault coefficient matrices with each entry belonging to $[0, 1]$, $\boldsymbol{\phi}_r = [\phi_{r1}, \phi_{r2}, \cdots, \phi_{rN}]^T$ and $\boldsymbol{\phi}_t = [\phi_{t1}, \phi_{t2}, \cdots, \phi_{tM}]^T$ are the additive fault vectors. Note that the normal actuator state without fault corresponds to the case of $\boldsymbol{\Upsilon}_r = \boldsymbol{I}_N$, $\boldsymbol{\phi}_r = \boldsymbol{0}_N$ and $\boldsymbol{\Upsilon}_t = \boldsymbol{I}_M$, $\boldsymbol{\phi}_t = \boldsymbol{0}_M$.

Since each control force component f_j, $j = 1, 2, \cdots, M$ is generated by a pair of symmetrical thrusters, we next make clear how they work together to generate the corresponding control force. In particular, along the assembling axis, one thruster generates a forward force T_j while the other generates a backward force H_j. Note that these two thrusters operate asynchronously in a normal case. Thus, when the actuator fault is concerned, the force component is expressed by

$$f_j = T_j - H_j \quad j = 1, 2, \cdots, M, \tag{A10}$$

where

$$\begin{cases} T_j = \upsilon_{tj}^t T_j^c + \phi_{tj}^t,\ H_j = 0, & \text{if } p_{tj} \geqslant 0, \\ H_j = -\upsilon_{tj}^h H_j^c + \phi_{tj}^h,\ T_j = 0, & \text{if } p_{tj} < 0, \end{cases} \tag{A11}$$

T_j^c, H_j^c are the command forces, $\upsilon_{tj}^t \in [0, 1]$, $\upsilon_{tj}^h \in [0, 1]$ are the fault coefficients, and ϕ_{tj}^t, ϕ_{tj}^h are the additive faults. By comparing (A9) and (A10), we know that

$$\begin{cases} T_j^c = p_{tj},\ H_j^c = 0, & \text{if } p_{tj} \geqslant 0, \\ H_j^c = -p_{tj},\ T_j^c = 0, & \text{if } p_{tj} < 0, \end{cases} \tag{A12}$$

and

$$\upsilon_{tj} = \begin{cases} \upsilon_{tj}^t, & \text{if } p_{tj} \geqslant 0, \\ \upsilon_{tj}^h, & \text{if } p_{tj} < 0, \end{cases}\ \phi_{tj} = \begin{cases} \phi_{tj}^t, & \text{if } p_{tj} \geqslant 0, \\ \phi_{tj}^h, & \text{if } p_{tj} < 0, \end{cases} \tag{A13}$$

which implies that the potential faults of a pair of thrusters are not identical. Moreover, (A11) also indicates that only one thruster in each pair works at a moment depending on the sign of the corresponding command force.

Remark 1. In this paper, we consider the actual physical actuators that are commonly used in spacecraft. In particular, momentum wheels and pairs of thrusters generate the control torque and force, respectively. Also, the faulted torque and force herein are specified directly with respect to these actual physical actuators. Moreover, according to (A12) and (A13), it can be verified that $\upsilon_{tj}p_{tj}$ is continuous since $\lim_{p_{tj}\to 0^+}(\upsilon_{tj}^t p_{tj}) = \lim_{p_{tj}\to 0^-}(\upsilon_{tj}^h p_{tj}) = 0$.

Define $\boldsymbol{x} = [\tilde{\boldsymbol{\sigma}}^T, \tilde{\boldsymbol{r}}^T]^T$ and $\boldsymbol{z} = [\tilde{\boldsymbol{\omega}}^T, \tilde{\boldsymbol{v}}^T]^T$. In terms of (A4) and (A6)–(A9), the six-dof error dynamics can be derived as

$$\dot{\boldsymbol{x}} = \boldsymbol{\Gamma}\boldsymbol{z}, \tag{A14}$$

$$\boldsymbol{M}\dot{\boldsymbol{z}} = \boldsymbol{\varsigma} + \boldsymbol{A}\boldsymbol{\Upsilon}\boldsymbol{p} + \boldsymbol{d}, \tag{A15}$$

where $\boldsymbol{\Gamma} = \mathrm{diag}(\boldsymbol{G}(\tilde{\boldsymbol{\sigma}}), \boldsymbol{I}_3)$, $\boldsymbol{M} = \mathrm{diag}(\boldsymbol{J}, m\boldsymbol{I}_3)$, $\boldsymbol{\varsigma} = [\boldsymbol{\varsigma}_r^T, \boldsymbol{\varsigma}_t^T]^T$ with $\boldsymbol{\varsigma}_r = -\boldsymbol{\omega}^\times\boldsymbol{J}\boldsymbol{\omega} + \boldsymbol{J}(\tilde{\boldsymbol{\omega}}^\times\tilde{\boldsymbol{R}}\boldsymbol{\omega}_d - \tilde{\boldsymbol{R}}\dot{\boldsymbol{\omega}}_d)$ and $\boldsymbol{\varsigma}_t = -m\boldsymbol{C}_t\boldsymbol{v} - m\boldsymbol{n}_t - m\ddot{\boldsymbol{\delta}}$, $\boldsymbol{A} = \mathrm{diag}(\boldsymbol{A}_r, \boldsymbol{R}_L^B\boldsymbol{A}_t)$, $\boldsymbol{\Upsilon} = \mathrm{diag}(\boldsymbol{\Upsilon}_r, \boldsymbol{\Upsilon}_t)$, $\boldsymbol{p} = [\boldsymbol{p}_r^T, \boldsymbol{p}_t^T]^T$, and $\boldsymbol{d} = [\boldsymbol{d}_r^T, \boldsymbol{d}_t^T]^T$ with $\boldsymbol{d}_r = \boldsymbol{A}_r\boldsymbol{\phi}_r + \boldsymbol{\tau}_d$ and $\boldsymbol{d}_t = \boldsymbol{B}\boldsymbol{\phi}_t + \boldsymbol{f}_d$.

Remark 2. In practical applications, the spatial disturbances usually arise from gravitation, solar radiation pressure, and other environmental factors which are always bounded in aerospace. Due to the fuel consumption of spacecraft, the inertia parameters are time-varying with limited changing rates. Thus, Assumption 1 is reasonable. Moreover, based on the full row rank of distribution matrix $\boldsymbol{A}_i$ and semi-positive definiteness of fault coefficient matrix $\boldsymbol{\Upsilon}_i$, $\inf\{\lambda_{\min}(\boldsymbol{A}_i\boldsymbol{\Upsilon}_i\boldsymbol{A}_i^T)\} > 0$, $i = r, t$ could guarantee the full-actuated condition of the control system. This implies that there are no more than $N-3$ torque and $M-3$ force actuators that totally fail at the same time. Zero eigenvalue of $(\boldsymbol{A}_i\boldsymbol{\Upsilon}_i\boldsymbol{A}_i^T)$ existing indicates that there is no actual control generated by actuators in the corresponding control axis. Therefore, Assumption 2 is also reasonable.

Appendix B Proof of Theorem 1

Define the estimate errors $\tilde{\zeta}_i = \hat{\zeta}_i - \zeta_i$ and $\tilde{\vartheta}_i = \hat{\vartheta}_i - \vartheta_i$, $i = r, t$. Choose the following Lyapunov function

$$V = \frac{1}{2}\boldsymbol{\xi}^T\boldsymbol{\xi} + \frac{1}{2}\boldsymbol{s}^T\boldsymbol{M}\boldsymbol{s} + \sum_{i=r,t}\Big(\frac{1}{2\beta_{i1}}\tilde{\zeta}_i^2 + \frac{1}{2\beta_{i2}}\eta_i\tilde{\vartheta}_i^2\Big). \tag{B1}$$

Its time derivative along the closed-loop trajectories can be given by

$$\begin{aligned}\dot{V} =&\boldsymbol{\xi}^T\dot{\boldsymbol{\xi}} + \boldsymbol{s}^T(\boldsymbol{M}\dot{\boldsymbol{s}} + \frac{1}{2}\dot{\boldsymbol{M}}\boldsymbol{s}) + \sum_{i=r,t}\Big(\frac{1}{\beta_{i1}}\tilde{\zeta}_i\dot{\tilde{\zeta}}_i + \frac{1}{\beta_{i2}}\eta_i\tilde{\vartheta}_i\dot{\tilde{\vartheta}}_i\Big)\\
=&-\boldsymbol{\xi}^T\boldsymbol{K}_1\boldsymbol{\xi} + \boldsymbol{\xi}^T\boldsymbol{\Theta}\boldsymbol{\Gamma}\boldsymbol{s} + \boldsymbol{s}^T\Big(\boldsymbol{\varsigma} + \boldsymbol{d} - \boldsymbol{M}\dot{\boldsymbol{\alpha}} + \frac{1}{2}\dot{\boldsymbol{M}}\boldsymbol{s}\Big) - \boldsymbol{A}\boldsymbol{\Upsilon}\boldsymbol{K}_2\boldsymbol{A}^T\boldsymbol{s} + \sum_{i=r,t}\Big(\frac{1}{\beta_{i1}}\tilde{\zeta}_i\dot{\hat{\zeta}}_i + \frac{1}{\beta_{i2}}\eta_i\tilde{\vartheta}_i\dot{\hat{\vartheta}}_i\Big)\\
=&-\boldsymbol{\xi}^T\boldsymbol{K}_1\boldsymbol{\xi} + \boldsymbol{\xi}_r^T\boldsymbol{\Theta}_r\boldsymbol{G}(\tilde{\boldsymbol{\sigma}})\boldsymbol{s}_r + \boldsymbol{\xi}_t^T\boldsymbol{\Theta}_t\boldsymbol{s}_t + \boldsymbol{s}^T\Big(\boldsymbol{\varsigma} + \boldsymbol{d} - \boldsymbol{M}\dot{\boldsymbol{\alpha}} + \frac{1}{2}\dot{\boldsymbol{M}}\boldsymbol{s}\Big) - (\kappa_r + \chi_r)\hat{\vartheta}_r\boldsymbol{s}_r^T\boldsymbol{A}_r\boldsymbol{\Upsilon}_r\boldsymbol{A}_r^T\boldsymbol{s}_r\\
&-(\kappa_t + \chi_t)\hat{\vartheta}_t\boldsymbol{s}_t^T\boldsymbol{R}_L^B\boldsymbol{A}_t\boldsymbol{\Upsilon}_t\boldsymbol{A}_t^T(\boldsymbol{R}_L^B)^T\boldsymbol{s}_t + \sum_{i=r,t}\Big(\frac{1}{\beta_{i1}}\tilde{\zeta}_i\dot{\hat{\zeta}}_i + \frac{1}{\beta_{i2}}\eta_i\tilde{\vartheta}_i\dot{\hat{\vartheta}}_i\Big)\end{aligned} \tag{B2}$$

According to Assumptions 1 and 2, it follows that

$$\Big\|\boldsymbol{\xi}_r^T\boldsymbol{\Theta}_r\boldsymbol{G}(\tilde{\boldsymbol{\sigma}})\boldsymbol{s}_r + \boldsymbol{\xi}_t^T\boldsymbol{\Theta}_t\boldsymbol{s}_t + \boldsymbol{s}^T(\boldsymbol{\varsigma} + \boldsymbol{d} - \boldsymbol{M}\dot{\boldsymbol{\alpha}} + \frac{1}{2}\dot{\boldsymbol{M}}\boldsymbol{s})\Big\| \leqslant \sum_{i=r,t}\zeta_i\|\boldsymbol{\psi}_i\|\|\boldsymbol{s}_i\|. \tag{B3}$$

Thus, $\dot{V}$ can be further derived as

$$\dot{V} \leqslant -\kappa_1\boldsymbol{\xi}_r^T\boldsymbol{\xi}_r - \kappa_2\boldsymbol{\xi}_t^T\boldsymbol{\xi}_t + \sum_{i=r,t}\Big(\zeta_i\|\boldsymbol{\psi}_i\|\|\boldsymbol{s}_i\| - (\kappa_i + \chi_i)\hat{\vartheta}_i\eta_i\|\boldsymbol{s}_i\|^2 + \frac{1}{\beta_{i1}}\tilde{\zeta}_i\dot{\hat{\zeta}}_i + \frac{1}{\beta_{i2}}\eta_i\tilde{\vartheta}_i\dot{\hat{\vartheta}}_i\Big). \tag{B4}$$

By virtue of the fact that $\hat{\vartheta}_i\eta_i = (\vartheta_i + \tilde{\vartheta}_i)\eta_i = 1 + \tilde{\vartheta}_i\eta_i$, it further follows that

$$\begin{aligned}\dot{V} \leqslant&-\kappa_1\boldsymbol{\xi}_r^T\boldsymbol{\xi}_r - \kappa_2\boldsymbol{\xi}_t^T\boldsymbol{\xi}_t - \kappa_r\boldsymbol{s}_r^T\boldsymbol{s}_r - \kappa_t\boldsymbol{s}_t^T\boldsymbol{s}_t + \sum_{i=r,t}\tilde{\zeta}_i\Big(\frac{1}{\beta_{i1}}\dot{\hat{\zeta}}_i - \frac{\|\boldsymbol{\psi}_i\|^2\|\boldsymbol{s}_i\|^2}{\sqrt{\|\boldsymbol{\psi}_i\|^2\|\boldsymbol{s}_i\|^2 + \varepsilon_i(t)^2}}\Big)\\
&+\sum_{i=r,t}\eta_i\tilde{\vartheta}_i\Big(\frac{1}{\beta_{i2}}\dot{\hat{\vartheta}}_i - (\kappa_i + \chi_i)\|\boldsymbol{s}_i\|^2\Big) + \sum_{i=r,t}\zeta_i\varepsilon_i(t).\end{aligned} \tag{B5}$$

Next, substituting adaptation laws yields

$$\begin{aligned}\dot{V} \leqslant&-\kappa_1\boldsymbol{\xi}_r^T\boldsymbol{\xi}_r - \kappa_2\boldsymbol{\xi}_t^T\boldsymbol{\xi}_t - \kappa_r\boldsymbol{s}_r^T\boldsymbol{s}_r - \kappa_t\boldsymbol{s}_t^T\boldsymbol{s}_t\\
&+\sum_{i=r,t}\Big(\zeta_i\varepsilon_i(t) - \tilde{\zeta}_i(\hat{\zeta}_i - \zeta_{i0})\varphi_{i1}(t) - \eta_i\tilde{\vartheta}_i(\hat{\vartheta}_i - \vartheta_{i0})\varphi_{i2}(t)\Big).\end{aligned} \tag{B6}$$

It follows from Young's inequality that $-\tilde{\zeta}_i(\hat{\zeta}_i - \zeta_{i0})\varphi_{i1}(t) \leqslant -\frac{\varphi_{i1}(t)}{2}\tilde{\zeta}_i^2 + \frac{\varphi_{i1}(t)}{2}(\zeta_i - \zeta_{i0})^2$ and $-\eta_i\tilde{\vartheta}_i(\hat{\vartheta}_i - \vartheta_{i0})\varphi_{i2}(t) \leqslant -\frac{\varphi_{i2}(t)}{2}\eta_i\tilde{\vartheta}_i^2 + \frac{\varphi_{i2}(t)}{2}\eta_i(\vartheta_i - \vartheta_{i0})^2$. Thus, $\dot{V}$ further satisfies

$$\begin{aligned}\dot{V} \leqslant&-\kappa_1\boldsymbol{\xi}_r^T\boldsymbol{\xi}_r - \kappa_2\boldsymbol{\xi}_t^T\boldsymbol{\xi}_t - \kappa_r\boldsymbol{s}_r^T\boldsymbol{s}_r - \kappa_t\boldsymbol{s}_t^T\boldsymbol{s}_t\\
&+\sum_{i=r,t}\Big(\epsilon_i(t) + \zeta_i\varepsilon_i(t) + \frac{\varphi_{i1}(t)}{2}(\zeta_i - \zeta_{i0})^2 + \frac{\varphi_{i2}(t)}{2}\eta_i(\vartheta_i - \vartheta_{i0})^2\Big).\end{aligned} \tag{B7}$$

By integrating both sides of (B7), it follows that

$$\begin{aligned}&V(t) + \kappa_1\int_0^t\|\boldsymbol{\xi}_r(\tau)\|^2\mathrm{d}\tau + \kappa_2\int_0^t\|\boldsymbol{\xi}_t(\tau)\|^2\mathrm{d}\tau + \kappa_r\int_0^t\|\boldsymbol{s}_r(\tau)\|^2\mathrm{d}\tau + \kappa_t\int_0^t\|\boldsymbol{s}_t(\tau)\|^2\mathrm{d}\tau\\
\leqslant&V(0) + \sum_{i=r,t}\Big(\zeta_i\bar{\varepsilon}_i + \frac{\bar{\varphi}_{i1}}{2}(\zeta_i - \zeta_{i0})^2 + \frac{\bar{\varphi}_{i2}}{2}\eta_i(\vartheta_i - \vartheta_{i0})^2\Big) < \infty,\quad \forall t \geqslant 0.\end{aligned} \tag{B8}$$

This implies that $V, \tilde{\zeta}_i, \tilde{\vartheta}_i \in \mathcal{L}_\infty$[3] and $\boldsymbol{\xi} = [\boldsymbol{\xi}_r^T, \boldsymbol{\xi}_t^T]^T, \boldsymbol{s} = [\boldsymbol{s}_r^T, \boldsymbol{s}_t^T]^T \in \mathcal{L}_\infty \cap \mathcal{L}_2$[4]. According to the definition of transformation function, it thus follows that $-\underline{k}_j(t) < x_j(t) < \bar{k}_j(t)$, $\forall t \geqslant 0$ given that $\boldsymbol{\xi} \in \mathcal{L}_\infty$ and $-\underline{k}_j(0) < x_j(0) < \bar{k}_j(0)$, $j = 1, 2, \cdots, 6$. This indicates that the concerned transient performance maintenance is achieved. On the other hand, by virtue of the closed-loop dynamics, it is trivial to show that $\dot{\boldsymbol{\xi}}, \dot{\boldsymbol{s}} \in \mathcal{L}_\infty$. According to Barbalat's Lemma [4], it can be concluded that $\lim_{t\to\infty}\boldsymbol{\xi}(t) = 0$ and $\lim_{t\to\infty}\boldsymbol{s}(t) = 0$. From the definition of $\boldsymbol{\xi}$ and $\boldsymbol{s}$, it finally follows that $\lim_{t\to\infty}\boldsymbol{x}(t) = 0$ and $\lim_{t\to\infty}\boldsymbol{z}(t) = 0$.

Remark 3. It is interesting to note that the closed-loop performance can be tuned by adjusting the designed parameters in both performance function and control law. Careful analysis indicates that faster convergence time and convergence rate can be provided by smaller t_s and larger b, respectively. The smaller set of steady state error can be guaranteed by a smaller k_∞. Besides, larger control parameters $\boldsymbol{K}_1$ and $\boldsymbol{K}_2$ contribute to a faster convergence performance but larger control energy. To this end, a reasonable compromise should be made among practical requirements.

3) $\mathcal{L}_\infty = \{f(t)|\operatorname{ess\,sup}_{t\in\mathbb{R}^+}\|f(t)\| < \infty\}$

4) $\mathcal{L}_2 = \{f(t)|\int_0^\infty\|f(t)\|^2\mathrm{d}t < \infty\}$

Remark 4. Note from the virtual control $\boldsymbol{\alpha}$ that it is intricate to determine the analytical expression of the derivative of $\boldsymbol{\alpha}$. Instead, the Levant differentiator introduced in [5] is used to approximate $\dot{\boldsymbol{\alpha}}$:

$$\begin{cases} \dot{\boldsymbol{y}}_0 = -l_1 \mathrm{diag}\Big(|\boldsymbol{y}_0 - \boldsymbol{\alpha}|^{\frac{1}{2}}\Big)\mathrm{sign}(\boldsymbol{y}_0 - \boldsymbol{\alpha}) + \boldsymbol{y}_1, \\ \dot{\boldsymbol{y}}_1 = -l_2 \mathrm{sign}(\boldsymbol{y}_1 - \boldsymbol{\varrho}), \end{cases} \tag{B9}$$

where $\boldsymbol{y}_0$, $\boldsymbol{y}_1$ are the approximations of $\boldsymbol{\alpha}$ and $\dot{\boldsymbol{\alpha}}$, and l_1, l_2 are positive constants. According to [5], sufficiently large l_1 and l_2 guarantee high approximation accuracy in finite time.

Appendix C Numerical simulations

A specific scenario of a six-dof spacecraft tracking maneuver on an elliptical orbit is simulated in this section. The orbit parameters are supposed as follows: eccentricity $e = 0.001$, perigee altitude $r_{pa} = 400$km, orbit inclination $i_0 = \frac{\pi}{4}$, argument of perigee $\omega_0 = \frac{\pi}{6}$, right ascension of ascending node $\Omega_0 = \frac{5\pi}{18}$, earth radius $R_E = 6371$km, semimajor axis $a = \frac{r_{pa}+R_E}{1-e}$, and initial true anomaly $\nu(0) = \frac{\pi}{2}$. The desired angular velocity is $\boldsymbol{\omega}_d(t) = \frac{1.8}{\pi}\Big[\cos\Big(\frac{t}{40}\Big), -\sin\Big(\frac{t}{50}\Big), \cos\Big(\frac{t}{30}\Big)\Big]^T$ deg/s with initial attitude $\boldsymbol{\sigma}_d(0) = [0.1, 0.1, 0]^T$, and the desired trajectory is $\boldsymbol{\delta}(t) = \Big[200\cos\Big(\frac{\pi t}{600}\Big), 200\sin\Big(\frac{\pi t}{600}\Big), 0\Big]^T$m. Moreover, suppose that the spacecraft carries 4 momentum wheels with inertia momentum 0.0818kgm^2 and 4 pairs of thrusters. They are assembled with the distribution matrices $\boldsymbol{A}_r = \boldsymbol{A}_t = \Big[1, 0, 0, \frac{\sqrt{3}}{3}; 0, 1, 0, \frac{\sqrt{3}}{3}; 0, 0, 1, \frac{\sqrt{3}}{3}\Big]$. The faults of momentum wheels and thrusters are specified as follows

$$\begin{aligned}
v_{r1} =& 0.6 + 0.1e^{-0.5t} + 0.1\sin(0.05t) + 0.01\mathrm{rand}(0,1),\ v_{r2} = 0.7 + 0.1e^{-0.5t} + 0.12\cos(0.05t) + 0.02\mathrm{rand}(0,1),\\
v_{r3} =& 0,\ v_{r4} = 0.7 + 0.1e^{-0.5t} + 0.15\cos(0.05t) + 0.015\mathrm{rand}(0,1),\\
v_{t1}^t =& 0.65 + 0.12e^{-0.5t} + 0.01\mathrm{rand}(0,1),\ v_{t2}^t = 0,\\
v_{t3}^t =& 0.7 + 0.15e^{-0.5t} + 0.01\mathrm{rand}(0,1),\ v_{t4}^t = 0.8 + 0.1e^{-0.5t} + 0.01\mathrm{rand}(0,1),\\
v_{t1}^h =& 0.7 + 0.1e^{-0.5t} + 0.01\mathrm{rand}(0,1),\ v_{t2}^h = 0.45 + 0.12e^{-0.5t} + 0.01\mathrm{rand}(0,1),\\
v_{t3}^h =& 0.6 + 0.1e^{-0.5t} + 0.01\mathrm{rand}(0,1),\ v_{t4}^h = 0.6 + 0.15e^{-0.5t} + 0.01\mathrm{rand}(0,1),\\
\boldsymbol{\phi}_r =& 0.005\Big(1 + e^{-0.5t} + 0.7\sin\Big(\frac{\pi t}{150}\Big) + 0.6\cos\Big(\frac{\pi t}{150}\Big) + 0.02\mathrm{rand}(0,1)\Big) \times [1,1,0,1]^T,\\
\boldsymbol{\phi}_t^t =& 0.09\Big(0.9 + e^{-0.5t} + 0.6\sin\Big(\frac{\pi t}{75}\Big) + 0.4\cos\Big(\frac{\pi t}{75}\Big) + 0.01\mathrm{rand}(0,1)\Big) \times [1,0,1,1]^T,\\
\boldsymbol{\phi}_t^h =& 0.075\Big(1 + e^{-0.5t} + 0.4\sin\Big(\frac{\pi t}{75}\Big) + 0.5\cos\Big(\frac{\pi t}{75}\Big) + 0.01\mathrm{rand}(0,1)\Big) \times [1,0,1,1]^T,
\end{aligned}$$

where rand$(0,1)$ is defined as a random function satisfying the norm distribution with mean deviation 0 and standard deviation 1. Moreover, the inertia parameters of the spacecraft are chosen as $\boldsymbol{J} = \mathrm{diag}(4 + 0.35e^{-0.01t} + 0.012\mathrm{rand}(0,0.5), 4 + 0.337e^{-0.01t} + 0.01\mathrm{rand}(0,0.5), 3.84 + 0.5568e^{-0.01t} + 0.018\mathrm{rand}(0,0.5))$kgm^2 and $m = 20 + 2e^{-0.02t} + 0.1\mathrm{rand}(0,0.5)$kg. The spatial disturbances are supposed to be

$$\boldsymbol{\tau}_d = 0.001 \times \begin{bmatrix} 6 + 5\sin(\frac{\pi t}{150}) + 3.5\cos(\frac{\pi t}{150}) + 1.5\mathrm{rand}(0,1) \\ 5 + 4\sin(\frac{\pi t}{150}) + 4\cos(\frac{\pi t}{150}) + 1.2\mathrm{rand}(0,1) \\ 5 + 6\sin(\frac{\pi t}{150}) + 5\cos(\frac{\pi t}{150}) + 1.8\mathrm{rand}(0,1) \end{bmatrix} \mathrm{Nm},\ \boldsymbol{f}_d = 0.01 \times \begin{bmatrix} 6 + 5\sin(\frac{\pi t}{150}) + 3.5\cos(\frac{\pi t}{150}) + 1.5\mathrm{rand}(0,1) \\ 5 + 4\sin(\frac{\pi t}{150}) + 4\cos(\frac{\pi t}{150}) + 1.2\mathrm{rand}(0,1) \\ 5 + 6\sin(\frac{\pi t}{150}) + 5\cos(\frac{\pi t}{150}) + 1.8\mathrm{rand}(0,1) \end{bmatrix} \mathrm{N}.$$

The system states and estimates are initialized as $\boldsymbol{\sigma}(0) = [0.25, -0.3, 0.15]^T$, $\boldsymbol{\omega}(0) = [0,0,0]^T$deg/s, $\boldsymbol{r}(0) = [400; 100; 22]^T$m, $\boldsymbol{v}(0) = [0,0,0]^T$m/s, $\hat{\zeta}_r(0) = 0.2$, $\hat{\zeta}_t(0) = 0.01$, $\hat{\vartheta}_r(0) = 9$ and $\hat{\vartheta}_t(0) = 9$. The performance function parameters are designed as $\rho_{01} = 0.3$, $\rho_{02} = 0.45$, $\rho_{03} = 0.35$, $\rho_{04} = 230$, $\rho_{05} = 130$, $\rho_{06} = 30$, $\rho_{\infty 1} = \rho_{\infty 2} = \rho_{\infty 3} = 0.005$, $\rho_{\infty 4} = \rho_{\infty 5} = \rho_{\infty 6} = 0.5$, $\iota_1 = \iota_2 = \iota_3 = 0.4$, $\iota_4 = \iota_5 = \iota_6 = 0.5$, $b_1 = b_2 = b_3 = 0.08$, $b_4 = b_5 = b_6 = 0.005$, $t_1 = t_2 = t_3 = 60$s, $t_4 = t_5 = t_6 = 360$s, and $n = 2$. In addition, the control parameters are selected as $\kappa_1 = 0.08$, $\kappa_2 = 0.08$, $\kappa_3 = 0.01$, $\kappa_4 = 0.01$, $\beta_1 = 0.1$, $\beta_2 = 0.1$, $\beta_3 = 0.001$, $\beta_4 = 0.1$, $\varepsilon_r = 0.01e^{-0.0001t}$, $\varepsilon_t = 0.05e^{-0.001t}$, $\varphi_1 = 0.01e^{-0.01t}$, $\varphi_2 = 0.01e^{-0.01t}$, $\varphi_3 = 0.01e^{-0.01t}$ and $\varphi_4 = 0.01e^{-0.01t}$. Furthermore, to evaluate the performance of the proposed control strategy (labeled by Proposed), a comparison with an adaptive controller [6] (labeled by AD) with fault compensating algorithm [7] is also given. The simulation results are illustrated in Figures C1-C5.

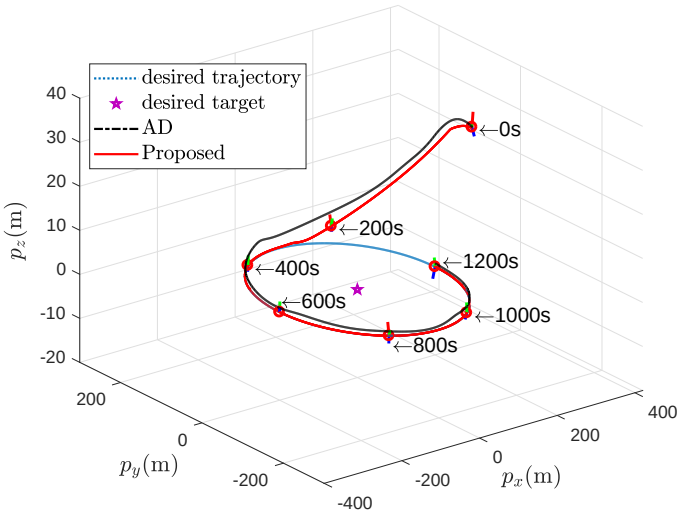

Figure C1 Trajectory in the LVLH frame.

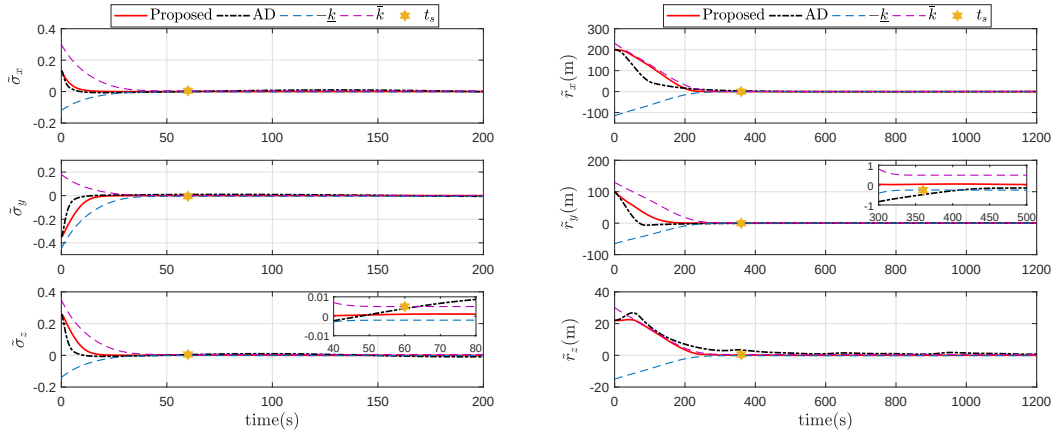

Figure C2 Attitude and position tracking errors.

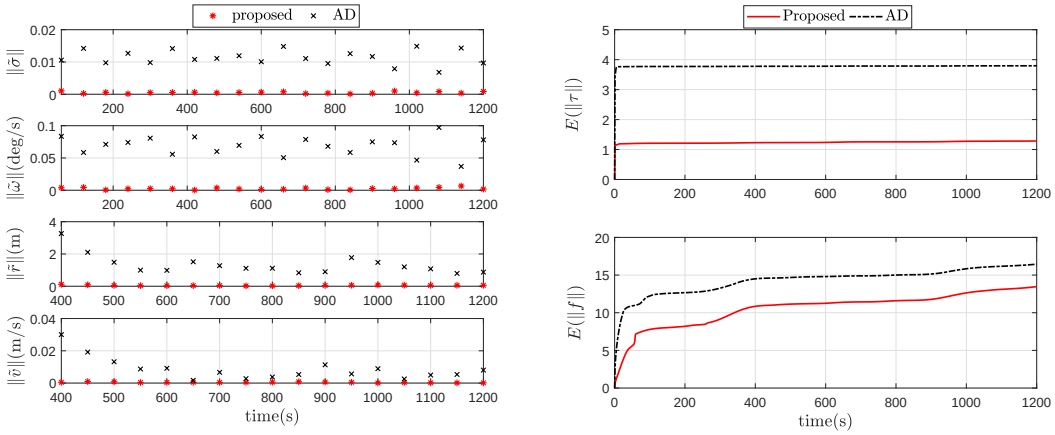

Figure C3 Energy index $E(\boldsymbol{u})$.

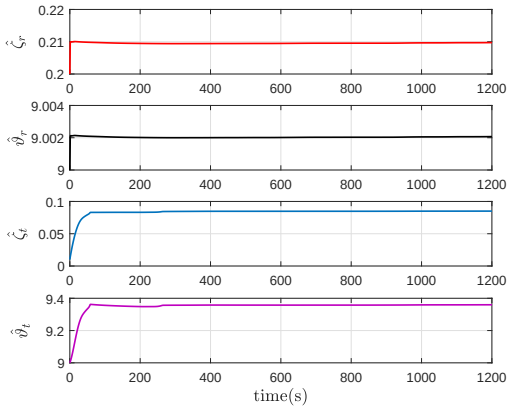

Figure C4 The estimates of parameter.

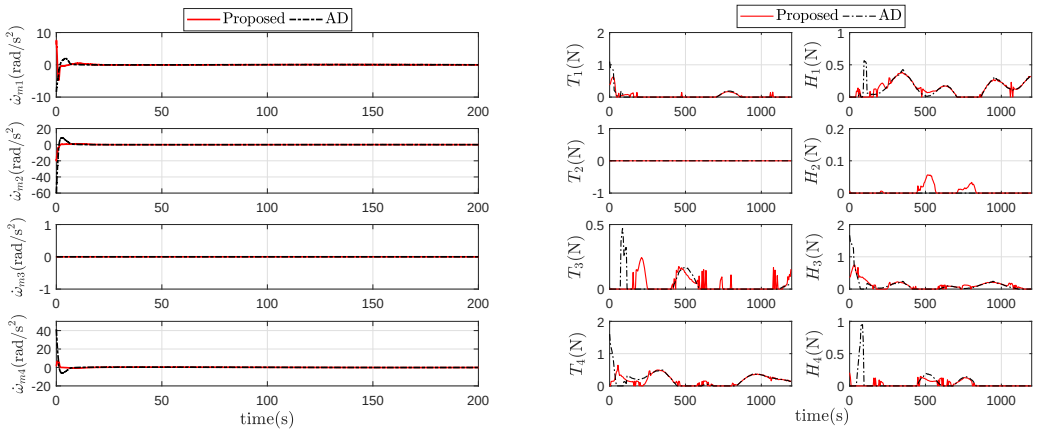

Figure C5 Actual control of thruster.

Figure C1 illustrates the trajectories of spacecrafts in the LVLH frame under different controllers. Figure C2 shows the snapshots of the attitude and position tracking errors. It can be observed from these figures that all the control strategies are able to achieve the tracking objective with good performance. It is clearly shown that the tracking errors converge to the preassigned sets with settling times 60s and 360s by using the proposed strategy, respectively. However, in contrast to the adaptive control strategy in [6] with fault compensating method [7] which violates the transient performance constraint, the proposed one realizes the six-dof spacecraft tracking while preserving the attitude and orbit errors within the prescribed constraints. By comparison, the proposed control strategy is more capable of maintaining the transient performance than the adaptive fault-tolerant control strategy [6, 7]. In addition, for a more illustrative comparison, some performance parameters resulting from two control strategies are given in Figure C3, where the control energy index $E(\boldsymbol{u})$ is defined as $E(\boldsymbol{u}) = \sqrt{\int_0^T \|\boldsymbol{u}(t)\|^2 \mathrm{d}t}$. The comparison results indicate that the proposed control strategy achieves the designated tracking objective with smaller control energy and smaller convergence errors in spite of disturbances, uncertain inertia parameters and actuator faults. On the other hand, it can be seen from Figure C4 that the parameter estimates are bounded. Finally, Figure C5 collects all the actual control signals of the torque and force actuators. In particular, T_2 of the thruster pair 2 is totally failed while H_2 is partially failed. It can be observed that there are no controls for T_2 and H_2 by using the fault compensating method [7] and H_2 still works by using the proposed strategy. Since there is no control command for H_2 under the method in [7], H_4 has to provide much more control to achieve the tracking maneuver. By comparison, the proposed strategy could contribute to a better working efficiency with less energy consumption.

References

1 Schaub H, Junkins J L. Analytical mechanics of space systems. AIAA Education Series, AIAA, Reston, VA, 2003.
2 Kristiansen R, Grotli E I, Nicklasson P J, et al. A model of relative translation and rotation in leader-follower spacecraft formations. Modeling, Identification and Control, 2007, 28(1): 3-13.
3 Sidi M J. Spacecraft Dynamics and Control: A Practical Engineering Approach. Cambridge University Press, New York, 1997.
4 Slotine J J, Li W. Applied nonlinear control, Prentice-Hall, 1991.
5 Levant A. Higher-order sliding modes, differentiation and output feedback control. International Journal of Control, 2003, 76: 924–941.
6 Sun L, Huo W. 6-DOF Integrated Adaptive Backstepping Control for Spacecraft Proximity Operations. IEEE Transactions on Aerospace and Electronic Systems, 2015, 51(3): 2433-2443.
7 Xia K, Zou Y. Adaptive Saturated Fault-Tolerant Control for Spacecraft Rendezvous with Redundancy Thrusters. IEEE Transactions on Control Systems Technology, 2019, DOI: 10.1109/TCST.2019.2950399.